

Space-Time Video Super-resolution with Neural Operator

Yuantong Zhang, *Student Member, IEEE*, Hanyou Zheng, Daiqin Yang, Zhenzhong Chen, *Senior Member, IEEE*
Haichuan Ma, and Wenpeng Ding

Abstract—This paper addresses the task of space-time video super-resolution (ST-VSR). Existing methods generally suffer from inaccurate motion estimation and motion compensation (MEMC) problems for large motions. Inspired by recent progress in physics-informed neural networks, we model the challenges of MEMC in ST-VSR as a mapping between two continuous function spaces. Specifically, our approach transforms independent low-resolution representations in the coarse-grained continuous function space into refined representations with enriched spatiotemporal details in the fine-grained continuous function space. To achieve efficient and accurate MEMC, we design a Galerkin-type attention function to perform frame alignment and temporal interpolation. Due to the linear complexity of the Galerkin-type attention mechanism, our model avoids patch partitioning and offers global receptive fields, enabling precise estimation of large motions. The experimental results show that the proposed method surpasses state-of-the-art techniques in both fixed-size and continuous space-time video super-resolution tasks.

Index Terms—Video Super-resolution, Video frame interpolation, Neutral operator

I. INTRODUCTION

The rapid advancement of multimedia technology, especially in hardware devices, has resulted in the widespread availability of high-resolution (HR) and high-frame-rate video sequences. However, due to shooting conditions and storage device limitations, recorded videos are often stored with limited spatial resolution and frame rates. Space-time video super-resolution (ST-VSR) seeks to transform low-resolution and low-frame-rate videos to higher spatial and temporal resolutions simultaneously, finding broad applications across various domains [1], [2]. The independent execution of video frame interpolation (VFI) and video super-resolution (VSR) overlooks the inherent correlation between space and time. Therefore, recent research has shifted towards considering VFI and VSR as a unified space-time video super-resolution (ST-VSR) process. Some earlier methods [3], [4] often employ ConvLSTM [5] structures for propagating information across multiple frames and subsequently performing upsampling. More recently, to increase model adaptability, several continuous space-time video super-resolution methods [6]–[8] have been introduced. These methods allow input modulation from low frame rate and low resolution to produce arbitrary high frame rate and high-resolution outcomes.

Nevertheless, despite the considerable progress made by these methods, two critical challenges still need to be addressed: 1) *efficient MEMC*, 2) *the ability to handle extreme*

motion. Regarding the first challenge, existing solutions either handle alignment and temporal interpolation separately [3], [4], [9] for pre-existing frames and interpolated frames or introduce additional encoders [7], [8] or separate optical flow estimation module [10], [11] to aid in motion estimation. Such approaches often result in unnecessary duplication of motion estimation and compensation processes, diminishing overall efficiency. When addressing the second challenge, our experiments reveal that current methods still exhibit significant blurring during large motion events.

Neural operator (NO) [12] is a recent innovation in neural networks designed to solve partial differential equation (PDE) problems. The objective of NO is to learn mappings between two infinite-dimensional function spaces, which have been applied broadly in several domains [13]–[15]. Some recent studies have shown that some neural operators can learn the resolution-invariant solution [16] in the turbulent regime. These observations show remarkable similarities between PDE-solving problems and space-time video super-resolution tasks (As illustrated in Fig. 1). For instance, the viscosity map in 2D Navier-Stokes equations [17] for predicting turbulent flow can be likened to video frame interpolation. Certain NOs [16], [18], [19] have been found to possess resolution-independent characteristics, similar to a zero-shot super-resolution. This insight leads us to reframe the ST-VSR problem. Due to the inherent nature of the STVSR task, it needs to mine fine-grained representations containing rich inter-frame spatio-temporal information from coarse-grained features that only contain intra-frame information. These fine-grained representations will serve as input for the subsequent upsampling stage. Therefore, from the perspective of neural operators, our task is transformed into learning the mapping between two continuous function spaces with different spatio-temporal representation granularities. Under this framework, we introduce an ST-VSR neural operator (STNO) incorporating a Galerkin-type kernel integral to tackle the challenges above. Benefiting from the linear complexity of Galerkin-type attention, we do not perform any typical patch partition [20], [21] operators, which are widely adopted in transformer-based methods but directly estimate motion with a global receptive field. This significantly enhances the precision and efficiency of motion estimation, particularly with extreme motion. Moreover, the neural operator’s robust modeling capabilities allow for the consolidation of motion information for alignment and interpolation, thereby eliminating redundant MEMC calculations. Our contributions are outlined as follows:

- We model space-time video super-resolution as a neural operator learning task in two continuous function spaces. The space-time neural operator (STNO) learner aims at translating coarse-grained spatial data, containing only information within individual frames, into high-quality results that incorporate information across frames. The improved fine-grained representation can assist in achieving better spatiotemporal restoration.
- We propose a Galerkin-type attention mechanism for motion estimation and motion compensation (MEMC). Thanks to its linear complexity, we can efficiently perform MEMC with the global receptive field thus improving the accuracy and reliability of motion information, especially in cases involving fast and extreme motions.
- Extensive experiments demonstrate the proposed approach outperforms existing methods in both fixed and continuous ST-VSR tasks with faster speed and reduced parameters.

The rest of the paper is organized as follows: Section II reviews the relevant literature. Details of the proposed methodology is given in Section III. Experiments and analyses are provided in Section IV. Finally, conclude the paper in Section V.

II. RELATED WORK

A. Space-Time Video Super-Resolution

With the rapid development of deep learning, numerous video frame interpolation (VFI) [22]–[25] and video super-resolution (VSR) [26]–[30] methods have been proposed, continuously pushing the benchmark performance. Readers can refer to the surveys [31] and [32] for more detailed information. Since both VFI and VSR require the effective utilization of spatiotemporal information from multiple frames, the natural idea is to consider them as a joint task, referred to as space-time video super-resolution. As a representative approach, Zooming Slow-Mo [3] establishes a comprehensive framework that utilizes ConvLSTM to aggregate spatiotemporal information. Building upon the Zooming Slow-Mo, Xu *et al.* [4] introduce a temporal modulation network for controllable intermediate feature interpolation. To further enhance flexibility, recent work has begun to explore continuous space-time video super-resolution. Chen *et al.* [7] propose an arbitrary spatiotemporal video super-resolution framework called VideoINR, which enables continuous space-time upscaling. Most recently, MoTIF [8] replaces the backward warping module in VideoINR with forward warping, resulting in improved performance. Although previous approaches have made significant progress, there are still issues with the efficiency of multi-frame motion estimation and motion compensation, particularly in handling large motions, which can lead to problems such as blurry artifacts and temporal inconsistency.

B. Neural Operators

Neural operator [12] (NO) is first introduced to solve partial differential equation (PDE) problems. It approximates the mapping between two infinite-dimensional spaces with the composition of nonlinear activation functions and a specific

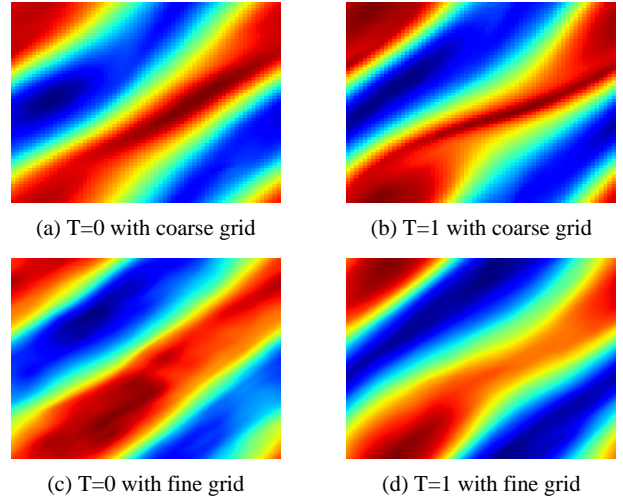


Fig. 1: Visualization of the Navier-Stokes equation problem, Physics-Informed Neural Operator (PINN) focuses on two main issues: (1) Sequence prediction problem: Given a time series of fluid fields as input, the neural operator aims to predict fluid changes for the next time interval. (e.g., (a) \rightarrow (b)). (2) Zero-shot super-resolution, which involves training on lower resolution data with coarse-grained discretization and evaluating on higher resolution data with fine-grained discretization. (e.g., Training: (a) \rightarrow (b), evaluation: (c) \rightarrow (d).)

class of integral operators. Based on previous work [12], the Fourier neural operator (FNO) is proposed by parameterizing the integral kernel directly in Fourier space. By utilizing the Fourier transform, FNO can model long-range information and capture spatial information over long distances with quasi-linear complexity. Cao *et al.* [33] introduce a novel integral operator that incorporates a modified attention mechanism. This Galerkin-type attention explicitly represents a Petrov-Galerkin projection and exhibits linear complexity attention without the softmax operation. Most recently, Wei *et al.* [34] propose utilizing NO to address the task of single image super-resolution. Although this method has demonstrated its superiority, exploring more efficient utilization for multi-frame image restoration with neural operators still needs to be explored. In reality, NOs are primarily employed to tackle time-related prediction problems; utilizing them solely to enhance intra-frame information fails to exploit the potential of neural operators fully. In light of this, our paper focuses on exploring more efficient and effective inter-frame MEMC.

III. METHODOLOGY

A. Problem Formulation

The concept of the neural operator was initially introduced in [12] intending to learn a mapping between infinite-dimensional spaces using a finite set of input-output data pairs. Generally, a typical neural operator consists of three components, and we borrow the language from [16] to provide a brief introduction. 1) Input projection: This component typically serves as a task-specific feature extractor that maps the data

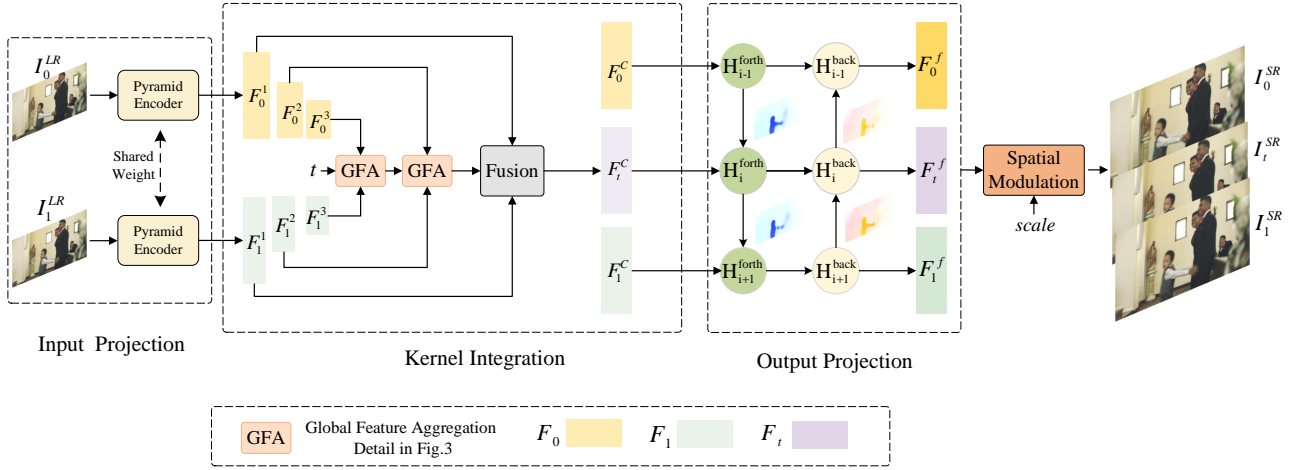


Fig. 2: Overview of the proposed method. We first extract multi-scale coarse-grained intra representations $F_{\{0,1\}}^{\{1,2,3\}}$, which a kernel-integrated operator subsequently processes to perform multi-scale MEMC. The obtained coarse-grained features F^c and motion information are further enhanced through multi-frame information propagation, resulting in fine-grained representations F^f , which contain rich spatiotemporal information. Finally, the obtained F^f are used for upsampling.

into a higher-dimensional space. 2) Kernel integral operator: This component extracts information from the input data, often exhibiting temporal correlations. As a result, sequential data modeling problems (e.g., Burgers' equation, Navier-Stokes equation) are commonly associated with transformers [35]. 3) Output projection: This component maps the data to the output feature space. In our work, the proposed STNO also consists of these three components, and each component has been designed with task-driven considerations. In contrast to PDE solving tasks that have well-defined physical backgrounds [16], [36], directly learning the operator from low resolution and low frame rate (LRLF) video to high resolution and high frame rate (HRHF) video is exceptionally challenging due to the highly nonlinear nature of real-world motion. We need to explore rich inter-frame spatiotemporal information from a video sequence for video super-resolution tasks. Therefore, we are not directly learning the mapping from LRLF to HRHF but rather from the input's coarse representations F^c to accurate representations F^f containing abundant spatiotemporal information. Let $D \subset \mathbb{R}^d$ be a bounded, open set and $\mathcal{A} = \mathcal{A}(D; \mathbb{R}^{d_a})$ and $\mathcal{U} = \mathcal{U}(D; \mathbb{R}^{d_u})$ be separable Hilbert spaces \mathcal{H} of function taking values in \mathbb{R}^{d_a} and \mathbb{R}^{d_u} . The input LRLF features and the corresponding fine-grained outputs are vector-valued functions within \mathcal{A} and \mathcal{U} , respectively. To work with them numerically, we access the discretized function values of input video at (x, y, t) through their corresponding spatial and temporal coordinate. Given sampled function pairs $\{a^k, u^k\}_{k=1}^N$ where $a^k \sim \mu$ is an i.i.d. sequence from the probability measure μ supported on \mathcal{A} , we introduce a neural operator $\mathcal{G}^\dagger : \mathcal{A} \rightarrow \mathcal{U}$, parametrized by θ , that aims to learn the mapping between two infinite dimensional space. In practice, the process of operator learning $\mathcal{G}^\dagger \leftarrow \mathcal{G}_\theta$ is often modeled as an empirical risk minimization problem which is the minimizer of discretized sampled observations u^k and a^k with the cost

function C :

$$\begin{aligned} \min_{\theta} \mathbb{E}_{a \sim \mu} \|C(\mathcal{G}(a, \theta) - \mathcal{G}^\dagger(a))\|, \\ \approx \min_{\theta} \frac{1}{N} \sum_{k=1}^N \|u^{(k)} - \mathcal{G}_\theta(a^{(k)})\|_{\mathcal{U}}, \end{aligned} \quad (1)$$

where a and u denote LRLF input features and corresponding representation with abundant spatiotemporal information. As [12], [16] shows, the operator \mathcal{G} is often modeled as an iterative architecture with dimension d_z . Then $\mathcal{G}_\theta : \mathcal{A} \rightarrow \mathcal{U}$ can be formulated as follows:

$$\begin{aligned} v_0(x) &= \mathcal{P}(x, a(x)), \\ v_{t+1}(x) &= \sigma(W_t v_t(x) + \mathcal{K}_t(v_t; \theta)(x)), \\ u(x) &= \mathcal{Q}(v_T(x)), \end{aligned} \quad (2)$$

where $\mathcal{P} : \mathbb{R}^{d_a+d} \rightarrow \mathbb{R}^{d_z}$, and $\mathcal{Q} : \mathbb{R}^{d_z} \rightarrow \mathbb{R}^{d_u}$ are the input and output projection functions respectively, mapping the input a to its hidden representation v_0 and the last layer hidden representation v_T back to the output function u . $W : \mathbb{R}^{d_z} \rightarrow \mathbb{R}^{d_z}$ is a point-wise linear transformation, and $\sigma : \mathbb{R}^{d_z} \rightarrow \mathbb{R}^{d_z}$ is the nonlinear activation function. $\mathcal{K}(a; \theta)$ is a kernel integral transformation parameterized by a neural network, mapping to the bounded operators on $\mathcal{U}(D, \mathbb{R}^{d_z})$. And the kernel integral operator in Eq. 2 can be formulated as:

$$\begin{aligned} (\mathcal{K}(a; \phi)v_t)(x) &= \int_D \mathcal{K}(x, y, a(x), a(y); \phi)v_t(y) dy, \\ \forall x \in D, \end{aligned} \quad (3)$$

where $\mathcal{K}_\phi : \mathbb{R}^{2(d+d_a)} \rightarrow \mathbb{R}^{d_z \times d_z}$ is a neural network with learnable parameter $\phi \in \Theta_{\mathcal{K}}$, $a(x), a(y)$ stands for the discrete sampled points corresponding to the spatial positions (x, y) . With the learned transformation \mathcal{G} , the coarse-grained representation corresponding to LRLF can be converted into fine-grained representations containing rich spatiotemporal information. And the next step is to modulate the fine-grained features using a learnable underlying function to the desired HRHF outputs.

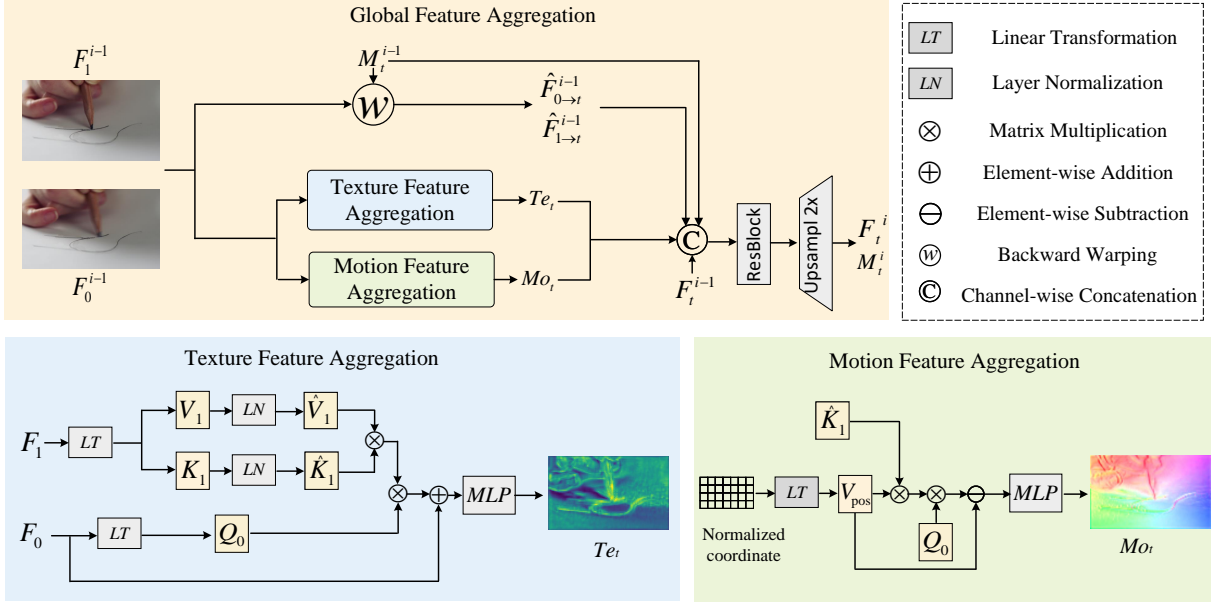


Fig. 3: The Global Feature Aggregation module comprises two main components: Texture Feature Aggregation and Motion Feature Aggregation. We employ a Galerkin-type attention mechanism to capture global texture features Te_t and motion features Mo_t . The generated Te_t and Mo_t are coupled together, mutually enhancing each other, ultimately resulting in high-quality interpolated intermediate frame features and motion flow.

B. Network Architecture

After the problem formulation, we introduce the specific network architecture, which is divided into three stages corresponding to Section III-A. Consider a video sequence consisting of N low-resolution images, which can be represented as a discretized vector-valued function $\mathcal{H} \ni f : \Omega \rightarrow \mathbb{R}^{N \times H \times W \times 3}$ containing only independent intra-frame information. We aim to use neural operators to extract fine-grained spatiotemporal representations that incorporate abundant inter-frame information. The framework of the proposed method is provided in Fig. 2.

Input Projection. Following some recent NO methods [33], [36], we first employ a stack of residual layers as a feature extractor to map the input data to a higher-dimensional space. Additionally, to capture multi-scale motion, we employ convolutions with a stride of 2 to obtain feature maps at three different resolutions concerning I_0 and I_1 , which we denote as $F_{\{i\}}^{\{j\}}$ ($i \in \{0, 1\}, j \in \{1, 2, 3\}$).

Kernel Integration. After obtaining the multi-scale features, we proceed to the kernel integration stage, where the goal is to extract motion information between adjacent frames and interpolate intermediate frames. Specifically, given the features F_0 and F_1 corresponding to the adjacent two frames, as well as the intermediate time step t , we aim to obtain the intermediate frame features F_t and the corresponding inter-frame motion information M_t . This process can be represented as:

$$M_t, F_t = \mathcal{K}(F_0, F_1, t), \quad (4)$$

where \mathcal{K}

represents the underlying kernel integral operator in Eq. 3, and M_t represents the inter-frame motion information. Specifically, since our task is spatiotemporal super-resolution, we

not only need the intermediate motion information $flow_{t \rightarrow 0,1}$ to fit the temporally interpolated frames but also require the motion information between pre-existing frames $flow_{0 \rightarrow 1,1 \rightarrow 0}$ for feature alignment.

Motion estimation for low-level vision tasks has been extensively studied for years. One persistent challenge is estimating large motions. The current state-of-the-art solutions often employ transformer [37], [38] architectures. However, vision transformers commonly suffer from quadratic computation and memory costs. Although patch partition operations [20], [39] can reduce complexity to some extent, they inevitably lead to limited receptive fields and suffer from blocking artifacts [40]. Inspired by recent advances in NO, we propose a global feature estimation module with linear complexity to address this issue, and the illustration is given in Fig. 3. Following the design of transformers, we use three learnable linear transformation matrices W_q , W_k , and W_v to multiply with the features to obtain the corresponding Query, Key, and Value:

$$Q_0 = F_0 \cdot W_Q, K_1 = F_1 \cdot W_K, V_1 = F_1 \cdot W_V. \quad (5)$$

Our goal is to use Q_0 to query K_1 and obtain similar appearances and motion information between I_0 and I_1 . To efficiently capture large motion, inspired by [33] we introduce a Galerkin-type attention mechanism that does not require softmax. It effectively replaces the traditional attention mechanism ($atten = softmax(\frac{QK^T}{\sqrt{d_z}})V$) and has linear computational complexity.

Consider an operator learning problem with an underlying domain $\Omega \subset \mathbb{R}^{n \times d_z}$, $\{x_i\}_{i=1}^n$ denotes the set of feature points in the discretized Ω . The columns of $Q/K/V$, respectively, contain the vector representations of the learned basis functions spanning certain subspaces of the latent representation

Hilbert spaces. Following settings in [33], we assume Q, K , and V are defined on the same spacial domain Ω with d_z dimensional vector-valued functions, with its subscript denoting the corresponding component. $k_l(\cdot)$, $v_j(\cdot)$ denote the vector representations of $k_l(1 \leq l \leq d_z)$ and v_j that evaluated at every sampled x_i . The kernel integral attention can be formulated as:

$$\begin{aligned} (\mathcal{K}(z)(x))_j &= \sum_{l=1}^{d_z} \langle v_j, k_l \rangle q_l(x) \quad \text{for } j = 1, \dots, d, \\ &\approx \sum_{l=1}^{d_z} \left(\int_{\Omega} v_j(\xi) k_l(\xi) d\xi \right) q_l(x_i), \forall x \in \Omega, \end{aligned} \quad (6)$$

in other words, this Galerkin-type attention of the output z can be then compactly written as:

$$z = \frac{Q_0(\hat{K}_1^T \hat{V}_1)}{n}. \quad (7)$$

In terms of the specific implementation process, given $Q_0, K_1, V_1 \in \mathbb{R}^{H \times W \times C}$, the texture feature Te_t is calculated as:

$$Te_t = MLP(F_0 + Q_0(\hat{K}_1^T \hat{V}_1)/(H \times W)), \quad (8)$$

where $\hat{K}_1 = LN(K_1), \hat{V}_1 = LN(V_1)$, and $LN(\cdot)$ denotes layer normalization operator, and MLP denotes the Multi-layer Perceptron. Unlike traditional attention mechanisms with quadratic complexity ($O((HW)^2C)$), this Galerkin-type attention exhibits only linear complexity ($O((HW)C^2)$), making it highly efficient. The detailed proof process can be found in [33]. Considering the alignment capability of the transformer [41] itself, Te_t actually integrates similar regions from I_0 and I_1 and adaptively fits the intermediate feature corresponding to time t . Like the process of modeling texture information, we model the motion information M_t similarly. First, we feed the normalized coordinate information into an MLP to modulate the positional information. Then, we estimate the motion information from I_0 to I_1 using inter-frame attention. The motion feature Mo_t is obtained by subtracting the original positional information from the motion representation that aggregates the pixel positional relationships between the two frames:

$$Mo_t = MLP(Q_0(\hat{K}_1^T V_{pos})/(H \times W) - V_{pos}), \quad (9)$$

where V_{pos} represents the normalized positional coordinates. Simultaneously, to gather more information and allow mutual enhancement between motion and texture, we perform both explicit (feature warping) and implicit (kernel integer operator) MEMC. As shown in Fig. 3, the feature aggregation and motion estimation are conducted in a coarse-to-fine pyramid manner. It means that the downsampled low-resolution features are first used to estimate coarse motion at smaller scales and gradually upsampled. The estimation results at the $(i-1)^{th}$ layer serve as guidance for the i^{th} layer, aligning with the iterative architecture of NO and the principle of residual learning.

Output Projection. After the kernel integral operation, we obtain temporally interpolated feature F_t , as well as the inter-frame motion flow M_t ($flow_{0 \rightarrow 1}, flow_{1 \rightarrow 0}, flow_{t \rightarrow 0}$, and

$flow_{t \rightarrow 1}$). The next step involves alignment within multiple frames to ensure that each frame receives supplementary information from the others (commonly called temporal propagation in video super-resolution). Here, we employ the popular bidirectional recurrent structure [28] to facilitate global propagation. Given a feature x_i corresponding to the i^{th} input LR, and the features propagated from its neighbors, denoted as H_{i-1}^f and H_{i+1}^b , we have:

$$\begin{aligned} H_i^b &= P_b(x_i, x_{i+1}, H_{i+1}^b), \\ H_i^f &= P_f(x_i, x_{i-1}, H_{i-1}^f), \\ \text{where } H_i^{b,f} &= \mathcal{W}(H_{i\pm 1}^{b,f}, M_i^{b,f}), \end{aligned} \quad (10)$$

where P_b and P_f denote the backward and forward propagation branches, and \mathcal{W} denotes backward warping. For the temporally interpolated frames, since the corresponding motion information $flow_{t \rightarrow 0}$ and $flow_{t \rightarrow 1}$ have also been computed, feature propagation is carried out similarly as with the originally available frames. Now, the feature representations for all frames contain rich spatiotemporal information and are ready for upsampling.

Spatial Modulation. The final step is to decode the feature as RGB values. To modulate the fine-grained spatiotemporal representations to arbitrary scales, we adopt a method similar to [42], where an MLP is used to predict the RGB values for each spatial position. Specifically, given the fine-grained spatiotemporal representation R_i corresponding to i^{th} frame and the associated coordinate position information $coord$, the super-resolution process can be represented as follows:

$$SR_i = MLP_s(R_i, coord), \quad (11)$$

where MLP_s denotes the underlying spatial modulation function. It is worth noting that, due to the powerful modeling capability of the neural operator, we only adopt local ensembling to aggregate the four nearest feature positions without the need for additional local feature unfolding operations [42] or feature aggregation [7], [8] process. It significantly reduces computational complexity and improves speed.

IV. EXPERIMENTS

A. Experiments Setup

Datasets. We use multiple datasets to train and test our model. The datasets we used are as follows:

Vime90k-T [47]: This dataset comprises 91,701 video clips, with each clip consisting of seven consecutive frames at a resolution of 448×256 . Following the approach in [3], [4], we divided the test set of Vimeo-90K-T into three subsets based on the average motion magnitude: fast, medium, and slow motion subsets.

Vid4 [48]: This dataset consists of four sequences and is characterized by rich textures. It is frequently used as a benchmark for video super-resolution.

Adobe [2]: It includes 17 test sequences captured at 240fps with an iPhone 6s. To align with the setup of VideoINR [7], we set the size of the temporal sliding window to 8 (i.e., 1^{st} , 9^{th} , 17^{th} , etc.) to generate the input LR frames and use them for interpolating the intermediate frames.

TABLE I: Quantitative comparisons of PSNR (dB), SSIM, speed (FPS), on Vid4, Vimeo-90K-T, GoPro and Adobe. The inference time is calculated on Vid4 dataset with one Nvidia 1080Ti GPU. † denotes only utilizing two adjacent images. For fairness, we calculate the speed using STNO-fix-two that takes two frames as input at a time. The best two results are highlighted in red and blue colors.

STVSR / VFI+VSR	Vid4		Vimeo-Fast		Vimeo-Medium		Vimeo-Slow		GoPro		Adobe		Speed FPS	Parameter
	PSNR	SSIM	PSNR	SSIM	PSNR	SSIM	PSNR	SSIM	PSNR	SSIM	PSNR	SSIM		
SuperSloMo [43]+Bicubic	22.84	0.5772	31.88	0.8793	29.94	0.8477	28.73	0.8102	27.50	0.8094	26.51	0.7650	-	19.8
SuperSloMo [43]+EDVR [44]	24.40	0.6706	35.05	0.9136	33.85	0.8967	30.99	0.8673	29.75	0.8589	28.97	0.8398	4.94	19.8+20.7
DAIN [22]+Bicubic	23.55	0.6268	32.41	0.8910	30.67	0.8636	29.06	0.8289	28.41	0.8299	27.35	0.7877	-	24.0
DAIN [22]+EDVR [44]	26.12	0.7836	35.81	0.9323	34.66	0.9281	33.11	0.9119	31.21	0.8904	30.80	0.8871	4.00	24.0+20.7
DAIN [22]+BasicVSR [28]	25.79	0.7711	35.07	0.9275	33.82	0.9211	32.08	0.8988	31.01	0.8878	30.59	0.8836	16.72	24.0+6.3
EDSC [45]+BasicVSR++ [46]	26.27	0.7900	35.80	0.9315	34.62	0.9277	33.20	0.9129	31.09	0.8880	30.68	0.8823	10.31	8.9+7.3
IFRnet [24]+BasicVSR++ [46]	26.36	0.7917	36.26	0.9358	34.80	0.9292	33.22	0.9126	31.31	0.8913	30.89	0.8861	8.93	19.7+7.3
RIFE [23]+BasicVSR++ [46]	26.37	0.7939	36.01	0.9337	34.64	0.9275	33.19	0.9122	31.17	0.8891	30.75	0.8833	7.25	20.9+7.3
Zooming SlowMo [3]	26.31	0.7976	36.81	0.9415	35.41	0.9361	33.36	0.9138	30.57	0.9031	30.29	0.8996	12.40	11.1
TMnet [4]	26.43	0.8016	37.04	0.9435	35.60	0.9380	33.51	0.9159	30.37	0.9027	30.12	0.8984	11.60	12.3
VideoINR† [7]	25.78	0.7753	33.95	0.9232	33.37	0.9214	31.71	0.8963	30.73	0.8850	30.21	0.8805	0.77	11.3
MoTIF† [8]	25.79	0.7745	35.01	0.9281	33.98	0.9235	32.11	0.8981	31.04	0.8877	30.63	0.8839	0.52	12.6
STNO-fix-two† (Ours)	25.94	0.7773	36.30	0.9365	34.80	0.9291	32.87	0.9060	31.20	0.8901	30.83	0.8865	17.23	9.37
STNO-fix (Ours)	26.73	0.8138	37.13	0.9447	35.61	0.9383	33.52	0.9160	32.06	0.9060	31.85	0.9073	-	9.37

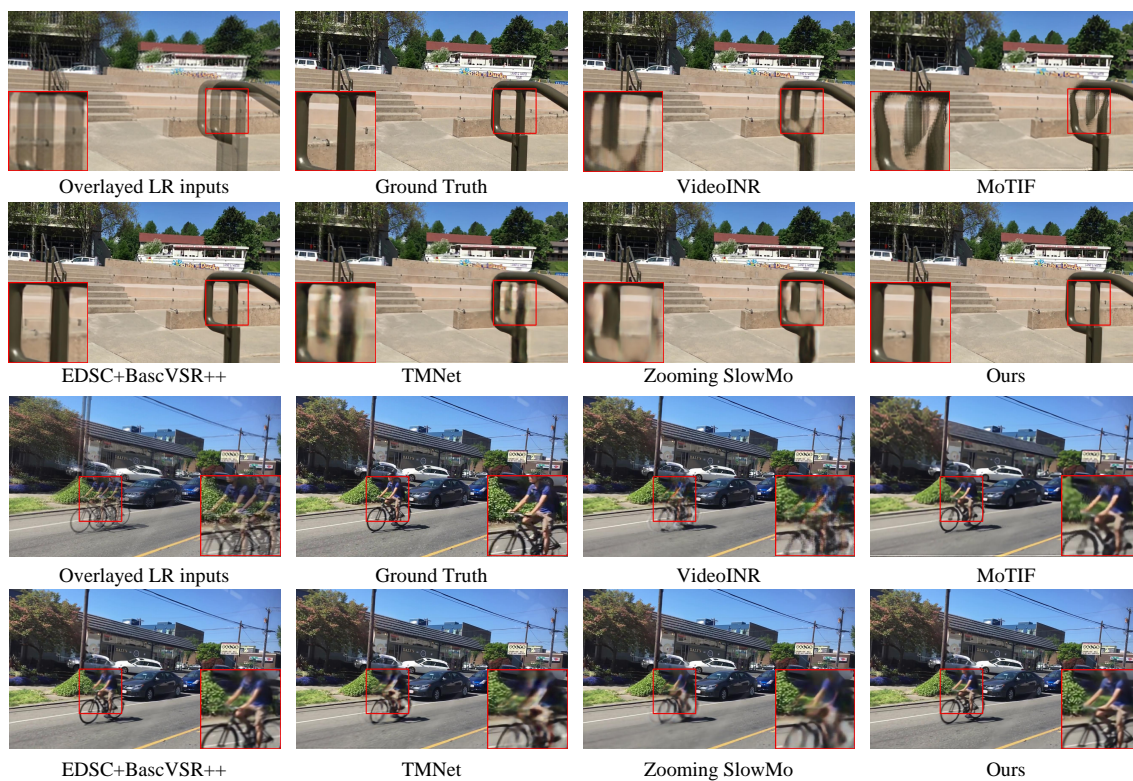


Fig. 4: Synthetic intermediate frame by different methods for large motion on Adobe. Pay attention to the areas outlined in red boxes, and zoom in for a better view.

GoPro [49]: It contains 11 videos of street scenes captured at high frame rates, presenting challenges associated with both object and camera motion.

SPMCS [50]: This dataset includes 32 videos and is widely used as a benchmark for video super-resolution. SPMCS exhibits rich textures and sensitivity to different scaling factors, making it suitable for evaluating the performance of continuous ST-VSR.

Implementation Details. We train two models to compare their performance for fixed spatiotemporal upsampling and continuous space-time super-resolution, which we refer to as "STNO-fix" and "STNO-c". To train STNO-fix, we crop

the images into 256×256 patches as the ground truth and downsample them by a factor of 4 using bicubic interpolation. The resulting frames, specifically the odd frames (e.g., 1^{st} , 3^{rd} , ...), are used as inputs to train the model. For model optimization, we employ the Adam optimizer [51] with $\beta_1=0.9$ and $\beta_2=0.999$. We also apply standard augmentation techniques, such as rotation, flipping, and random cropping. The initial learning rate was set to 2×10^{-4} and decayed to 1×10^{-7} using a cosine annealing scheduler. To facilitate longer information propagation, we adopted the approach described in [28], which involves applying temporal augmentation by flipping the original input sequence.

For the STNO-fix, the Vimeo-90K-T dataset [47] is em-

TABLE II: Quantitative comparison (PSNR (dB)/SSIM) of continuous space-time super-resolution. The results are calculated on SPMCS. The best results are highlighted in red.

Time Scale	Space Scale	TMnet	VideoINR	MoTIF	STNO-c (Ours)
×2	×2	-	30.67/0.9020	35.64/0.9663	38.55/0.9744
×2	×3	-	31.17/0.8959	31.38/0.9135	33.38/0.9245
×2	×4	29.23/0.8741	28.69/0.8430	28.94/0.8497	30.58/0.8620
×2	×5	-	28.05/0.7894	27.42/0.7934	28.73/0.8060
×2	×6	-	26.06/0.7361	26.33/0.7458	27.42/0.7579
×4	×2	-	30.10/0.8904	34.59/0.9470	36.62/0.9625
×4	×3	-	30.75/0.8870	31.17/0.9085	32.36/0.9127
×4	×4	28.02/0.8265	28.51/0.8373	28.88/0.8482	29.91/0.8512
×4	×5	-	27.94/0.7869	27.42/0.7942	28.30/0.7975
×4	×6	-	26.03/0.7359	26.37/0.7484	27.13/0.7517

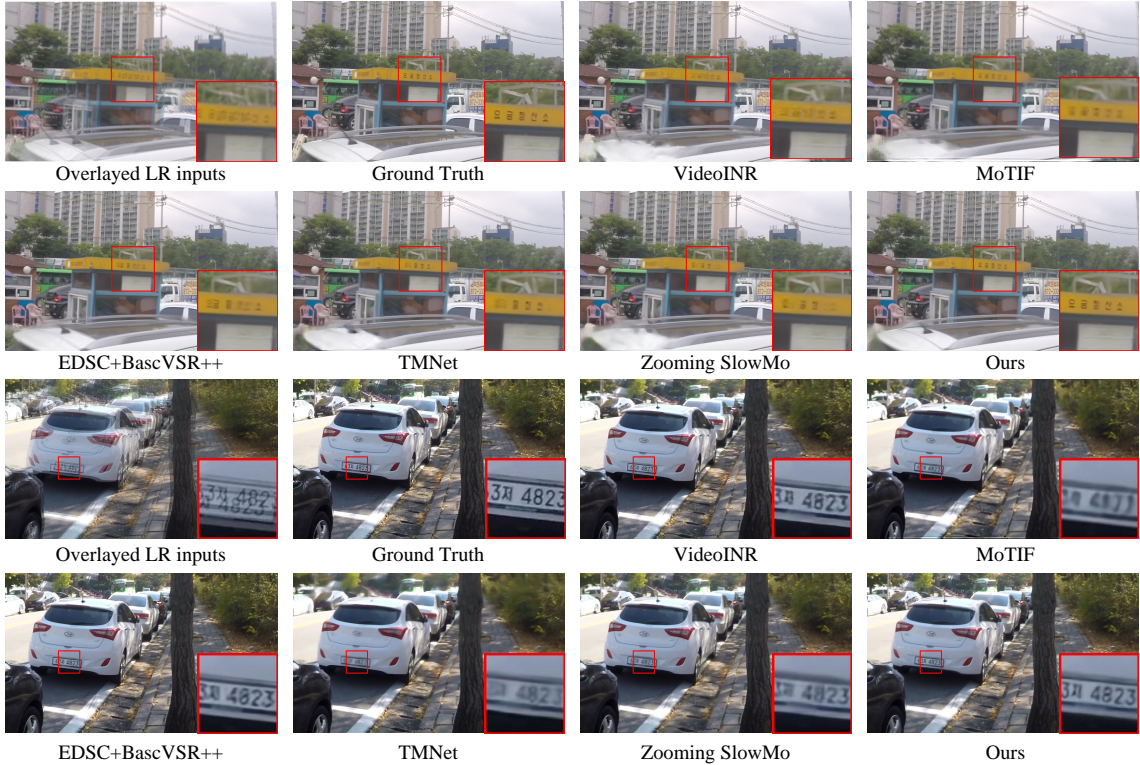


Fig. 5: Synthetic intermediate frame by different methods for large motion on Adobe. Pay attention to the areas outlined in red boxes, and zoom in for a better view.

ployed as the training set. We apply bicubic downsampling by a factor of 4 on odd-numbered frames (e.g., 1st, 3rd ...) as input, and corresponding high-resolution images (e.g., 1st, 2nd, 3rd ...) are used as supervision. We supervise both the pixel-wise predicted RGB pixel values using the Charbonnier loss [52] and the predicted motion flow simultaneously to better capture precise motion. The pseudo-labels for motion flow are obtained using a pre-trained optical flow model [53]. The loss function can be represented as follows:

$$\mathcal{L} = \mathcal{L}_{char}(\hat{I}_t^{SR}, I_t^{HR}) + \alpha \sum_{k=1}^3 \mathcal{L}_{char}(U_{2^k}(flow_k), flow_k), \quad (12)$$

where $\mathcal{L}_{char}(\hat{x}, x) = \sqrt{|\hat{x} - x|^2 + \varepsilon^2}$ denotes the Charbonnier loss [52], \hat{x} and x denotes the predicted results and their corresponding ground truth. ε is empirically set to 10^{-3} , U_s is

the bilinear upsampling operation with scale factor s , and α is a hyper-parameter, we set it to 10^{-2} . For STNO-c, to enable the model to have perception capabilities at different scales and arbitrary intermediate time, we follow TMNet [4] and perform generalization fine-tuning on Adobe [2] at multiple intermediate moments and scales. Specifically, we sampled the intermediate moment t from $\{1/8, 1/8, \dots, 7/8\}$ and the upscaling factors from $\{2.0, 2.2, \dots, 3.8, 4.0\}$ to train the STNO-c. The remaining experimental settings and training procedures are similar to those used for training the STNO-fix.

B. Comparisons to State-of-the-Arts

To evaluate the effectiveness of different super-resolution methods, we employ Peak Signal-to-Noise Ratio (PSNR) and



Fig. 6: Comparison of continuous video spatiotemporal super-resolution performance on the SPMCS dataset, where $S=A$ and $T=B$ indicate spatial upsampling by a factor of A and intermediate temporal moments of B .

structural similarity Index Measure (SSIM) as our performance metrics. Our comparative analysis encompasses both fixed and continuous Space-time video super-resolution methods.

Comparison for Fixed ST-VSR. Since the majority of existing methods are limited to fixed spatial and temporal interpolation scales for space-time upsampling, We first compare the results for space $4\times$ and time $2\times$ super-resolution with recent state-of-the-art one stage approaches [3], [4], [7], [8] and two-stage approaches that sequentially apply VFI [22]–[24], [43], [45] and VSR [28], [44], [46]. From Table I, it can be observed that the proposed method outperforms all other methods on all metrics across all datasets. We summarize the key points as follows: 1) The performance of the proposed method improves progressively as the motion magnitude and texture complexity of the datasets increases. Due to the lower resolution of the Vimeo-90k-T dataset, the performance improvement of our method is not significant. Nevertheless, when evaluated on more challenging datasets like Adobe and GoPro, our method outperforms all existing solutions by a significant margin, achieving approximately 1 dB higher PSNR than the second-best method. 2) Thanks to the inherent resolution-independent characteristics of the neural operator, our model demonstrates strong generalization capabilities. Despite being

trained only on Vimeo90k-T with lower resolution and smaller motion ranges, it achieves outstanding performance on both low-resolution and high-resolution data with varying motion ranges. In contrast, VideoINR [7] and MoTIF [8] exhibit significant performance degradation on Vimeo-90k-T, greatly limiting their adaptability to different scenarios. 3) Some methods like VideoINR and MoTIF only consider information from two adjacent frames, ignoring valuable information from distant frames. However, most videos consist of more than just two frames. Although we believe that this kind of evaluation approach is unreasonable, we still provide results using only two frames, which we refer to as "STNO-fix-two". It can be observed that even with only two frames, our results still outperform these approaches. 4) While achieving good flexibility, our method maintains the fastest speed and the smallest number of parameters. In comparison, VideoINR and MoTIF exhibit very slow inference speeds, as their complex additional motion encoding and feature aggregation components make their inference speed less than 1/10 of other approaches. In Fig. 4, we present the restoration results of different methods on the Adobe [2] dataset. It can be observed that due to the camera shake, there is significant motion between adjacent frames. Both deformable convolution kernels based [3], [4]

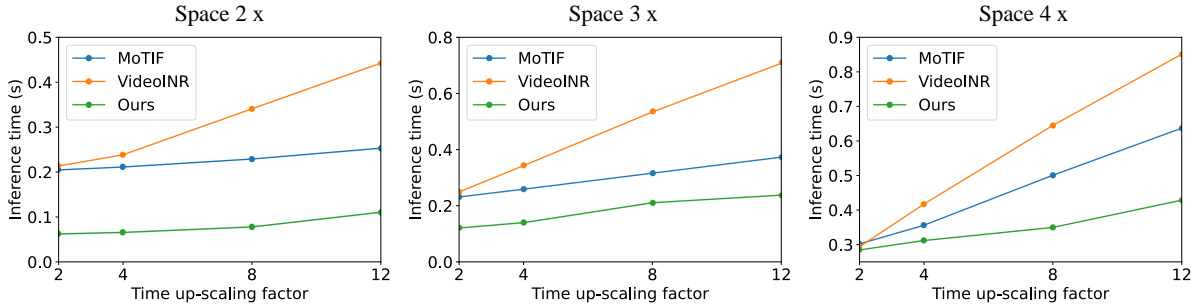


Fig. 7: Speed comparison of different continuous spatiotemporal super-resolution methods under various spatiotemporal upsampling rate combinations, our method outperforms the comparative algorithms in all tested cases. The input resolution is 128×128 , and the speed test was conducted on an NVIDIA 3090 GPU.

methods and optical based methods [7], [8] fail to produce visually pleasing intermediate frames. In the first set of comparisons, all end-to-end space-time video super-resolution methods exhibit severe artifacts in the region between the two pillars, indicating that these methods fail to correctly capture the corresponding pixels in two adjacent frames. In the second set of comparisons, results generated by VideoINR [7] and Zooming SloMo [3] exhibit noticeable ghosting effects between the bicyclist and the bicycle. Although TMNet [4] and MoTIF [8] produce relatively better results, there is still a considerable degree of blurring. When we play multiple video frames in succession, it causes quality jitter between frames, which affects the overall viewing experience. In contrast, some stronger two-stage methods (e.g., EDSC [45] + BasicVSR++ [46]) and our proposed method yield significantly superior results. When compared to two-stage methods, our approach not only produces relatively sharper and closer-to-ground-truth results but also maintains a smaller parameter count and faster inference speed. We also present two sets of comparative results on GoPro [49], where many scenes contain textual information. It can provide a good measure of the ability of different methods to maintain the continuity of texture patterns when synthesizing intermediate frames. As shown in Fig. 5, all other competing methods (whether two-stage or one-stage STVSR schemes) fail to effectively restore text information. In contrast, our method has successfully restored text that is clearer and more complete, with sharper edges, making it easier to recognize and also closer to the ground truth.

Comparison for Continuous ST-VSR. We then compare the results of continuous spatial-temporal upsampling. It has been noted in previous studies [7], [8] that a two-stage method involving sequential video frame interpolation and image super-resolution performs significantly poorer than a one-stage method. In this context, our focus is on comparing against end-to-end spatio-temporal super-resolution methods. Specifically, we compared different combinations of intermediate moments and resolutions. The experimental results are provided in Table II. It can be observed that our method significantly outperforms VideoINR and MoTIF, both for in-distribution and out-distribution results. In certain space-time combinations (e.g., $T \times 2$, $S \times 2$) the performance improvement reaches up to 3 dB. In Fig. 6, we present the visual comparison results

TABLE III: Evaluation for computational complexity (GFLOPs) on various datasets, we perform space $4 \times$ and time $2 \times$ upsampling. To accommodate certain methods that require the input image resolution to be a multiple of 8, we perform padding on the input image if needed.

Dataset	Vid	Vimeo	Adobe & GoPro	SPMCS
Input Size	144×184	64×112	184×320	128×240
VideoINR	924.85	250.20	2055.21	1072.29
MoTIF	1125.52	304.47	2501.32	1305.12
STNO (Ours)	543.03	146.91	1206.74	629.60

for different intermediate time steps and spatial resampling rate combinations. It can be seen that the proposed method exhibits significantly superior subjective visual quality, consistent with objective metrics. For instance, in the first set of images with $S=4$ and $T=0.5$, both VideoINR and MoTIF exhibit severe aliasing artifacts. In contrast, our method achieves superior inter-frame information alignment and restores more reliable texture details by leveraging abundant multi-frame information.

C. Computation Complexity Analysis

We carefully consider reducing the computational complexity in model design. Firstly, the Galerkin-type attention exhibits a linear complexity relationship with the input resolution. In contrast, many optical flow estimation networks [54]–[56] introduce correlation layers with quadratic complexity for motion estimation. Secondly, we have not designed a separate motion estimation module; instead, motion estimation and motion compensation are performed in a coupled manner. This compact design not only reduces the number of parameters but also enhances computational efficiency. On the contrary, some methods that introduce independent optical flow estimation networks often require additional post-processing modules (such as Gridnet in SoftSplat [57] or Unet in [38]) to reduce artifacts. Quantitative experiments also validate this point. In Fig. 7, we provide a speed comparison of various methods under different spatiotemporal super-resolution factors. It can be observed that the proposed approach achieves significantly faster inference speeds compared to VideoINR and MoTIF under all conditions. Additionally, Table III presents the GFLOPs of different methods on various test datasets. Our approach

TABLE IV: Ablation study of global texture aggregation and coupled MEMC. Quality metrics: PSNR(dB)/SSIM

Case	TFA	MFA	Vid	Adobe	GoPro
1	✗	✗	26.27/0.7977	30.02/0.8678	30.41/0.8769
2	✗	✓	26.37/0.7988	30.01/0.8659	30.44/0.8762
3	✓	✗	26.50/0.8052	31.01/0.8914	31.39/0.8954
4	✓	✓	26.72/0.8138	31.85/0.9073	32.06/0.9060

maintains the lowest floating point operations across different input resolutions, approximately half of the comparison methods. These experimental results demonstrate that the proposed approach not only achieves excellent performance but also significantly reduces computational complexity and inference time.

D. Visualization of Galerkin-type kernel Function

To better understand the working mechanism of Galerkin-type attention, we visualize the output of this module. As shown in Fig. 8, we present two consecutive frames and calculate the optical flow pseudo-label between the two frames using a state-of-the-art optical flow estimation model [53]. We also generate the normalized heatmap of attention (z in Eq 7). It can be observed that this module pays more attention to the regions with motion between the two frames. Additionally, z_0 focuses more on areas with significant motion, while z_1 emphasizes relatively subtle motion. This behavior arises from the iterative neural operator architecture, which allows the z_{i+1} motion estimation to effectively capture the residual motion from the z_i estimation.

E. Ablation Study

Global Feature Aggregation. As the most crucial part of this work, we craft a Galerkin-type attention including both texture feature aggregation (TFA) and motion feature aggregation (MFA) as the kernel function of the neural operator for global feature aggregation (GFA). Benefiting from the linear complexity presented by global feature aggregation for the input resolution, we do not need to perform any patch partition operations on the input features, which efficiently achieves a global receptive field. To validate the effectiveness of this module, we conduct an ablation study by omitting this mechanism and solely relying on optical flow warping for alignment purposes. The experimental results are presented in Table IV. It can be observed that removing the global MEMC (Case 1) results in severe performance degradation across all datasets. Specifically, the performance improvement brought by global feature aggregation is related to the characteristics of the dataset. Since the four sequences in the Vid dataset have relatively small motion ranges, the GFA module provides a modest improvement of around 0.45dB in terms of PSNR. However, for datasets with larger and more challenging motion ranges like Adobe and GoPro, the performance improvement is significant, reaching around 1.8 dB. In Fig. 9, we present two sets of typical visual results, each consisting of interpolated intermediate frames and their corresponding motion flow. It can be observed that when the attention mechanism is absent, it leads to a significant decrease in performance. In Table V, we

TABLE V: The impact of w/wo GFA on the quality of optical flow. We report the End Point Error (EPE) of predicted optical flows and their corresponding pseudo-labels.

	Vimeo-Slow	Vimeo-Medium	Vimeo-Fast	Vimeo-Avg
w/o GFA	0.43	0.96	2.87	1.15
w/ GFA	0.35	0.84	2.59	1.01
Difference	0.08	0.12	0.28	0.14

first utilize a state-of-the-art pre-trained optical flow extractor [53] to compute the optical flow for the Vimeo-90K-T dataset, which serves as pseudo-labels. Using these pseudo-labels, we then evaluate the model w/wo global feature aggregation based on the End Point Error (EPE). As shown, model with GFA significantly improves the accuracy of the optical flow estimation. Furthermore, the improvement becomes more apparent as the magnitude of motion increases.

Coupled MEMC. We perform progressive coupling estimation of texture and motion information using a Galerkin-type kernel, rather than designing a separate optical flow estimation module. The motivation behind coupled MEMC is as follows: at each spatial scale, more reliable texture information provides a smoother input for motion estimation, while more accurate motion information, in turn, helps synthesize more plausible intermediate frame textures. To validate the effectiveness of this mechanism, we retained only one of the two modules, TFA or MFA. (corresponding to Case 2 and Case 3 in Table IV). The results demonstrate that the absence of either module has a significant impact on performance. Another advantage of the coupled motion estimation is that we no longer need separate optical flow estimation modules (e.g., Spynet [58] for BasicVSR [28], Raft [55] for MoTIF [8]). This reduces the complexity of the model and allows motion information and texture information to promote each other, resulting in accurate alignment and more precise temporal interpolation.

V. CONCLUSIONS AND FUTURE WORK

In this paper, we present a novel approach to address the space-time video super-resolution (ST-VSR) task by formulating it as a neural operator learning problem. By conceptualizing the problem as a mapping between two function spaces, we aim to extract fine-grained spatiotemporal information from coarse-grained intra-frame features. Specifically, we adopt a Galerkin-type kernel integral in our neural operator, which enhances motion estimation’s precision and efficiency due to its global receptive field and linear complexity. Further, our model consolidates motion information for alignment and interpolation, eliminating redundant motion estimation and compensation calculations and enhancing overall efficiency. Extensive experiments demonstrate that our method outperforms state-of-the-art techniques in both fixed-size and continuous space-time video super-resolution tasks with faster speed and reduced parameter count.

Despite the significant improvements in performance and efficiency, there are still some limitations. Firstly, we focus on efficient and accurate motion estimation and compensation (MEMC), without explicitly considering the utilization of

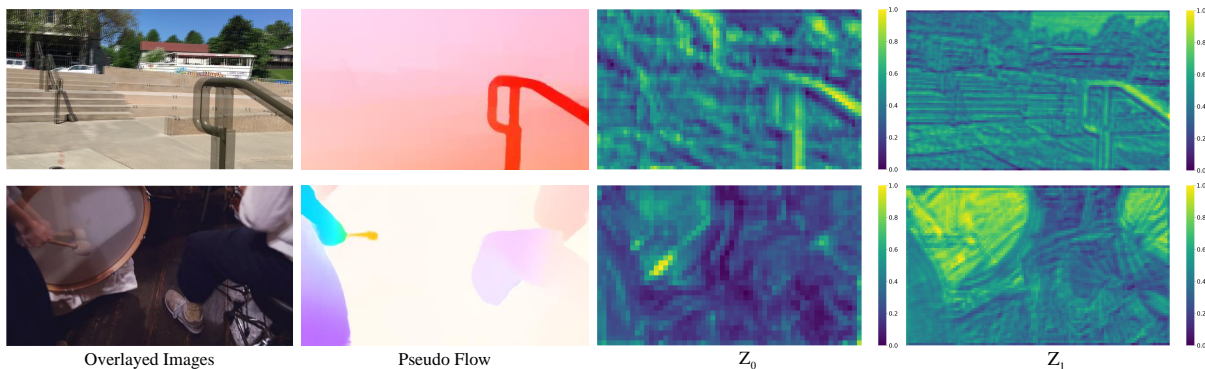


Fig. 8: Visual of the Galerkin type attention. From left to right, we display the overlapping consecutive frames, the pseudo-optical flow $flow_{0 \rightarrow 1}$ and the normalized output (z in Eq. 7) of the Galerkin-type attention module. Z_i represents the i^{th} iterative layer.

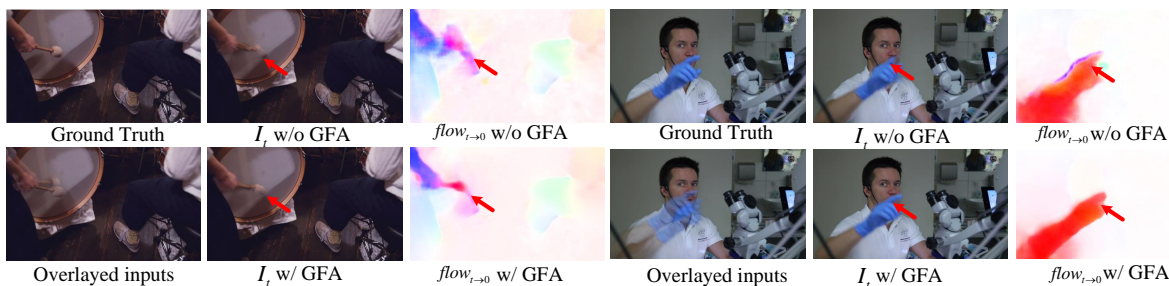


Fig. 9: Visual comparison of w/o Global Feature Aggregation (GFA) module. We also provide visualization results of the corresponding estimated motion flow.

intra-frame information. Furthermore, in our approach, the utilization of neural operator primarily focuses on addressing the MEMC problem. This is attributed to the inherent complexity of capturing real-world motion, which poses a challenge in establishing an end-to-end neural operator framework that directly achieves both temporal and spatial super-resolution. We leave these issues for future work.

REFERENCES

- [1] J. Flynn, I. Neulander, J. Philbin, and N. Snavely, “Deepstereo: Learning to predict new views from the world’s imagery,” in *IEEE Conference on Computer Vision and Pattern Recognition*, 2016, pp. 5515–5524.
- [2] S. Su, M. Delbracio, J. Wang, G. Sapiro, W. Heidrich, and O. Wang, “Deep video deblurring for hand-held cameras,” in *IEEE Conference on Computer Vision and Pattern Recognition*, 2017, pp. 237–246.
- [3] X. Xiang, Y. Tian, Y. Zhang, Y. Fu, J. P. Allebach, and C. Xu, “Zooming slow-mo: Fast and accurate one-stage space-time video super-resolution,” in *IEEE Conference on Computer Vision and Pattern Recognition*, 2020, pp. 3370–3379.
- [4] G. Xu, J. Xu, Z. Li, L. Wang, X. Sun, and M. Cheng, “Temporal modulation network for controllable space-time video super-resolution,” in *IEEE Conference on Computer Vision and Pattern Recognition*, 2021, pp. 6388–6397.
- [5] S. Kim, S. Hong, M. Joh, and S. K. Song, “Deeptrain: ConvLSTM Network for precipitation prediction using multichannel radar data,” *arXiv preprint arXiv:1711.02316*, 2021.
- [6] Z. Shi, X. Liu, C. Li, L. Dai, J. Chen, T. N. Davidson, and J. Zhao, “Learning for unconstrained space-time video super-resolution,” *IEEE Transactions on Broadcasting*, pp. 345–358, 2021.
- [7] Z. Chen, Y. Chen, J. Liu, X. Xu, V. Goel, Z. Wang, H. Shi, and X. Wang, “VideoINR: Learning video implicit neural representation for continuous space-time super-resolution,” in *IEEE Conference on Computer Vision and Pattern Recognition*, 2022, pp. 2047–2057.
- [8] Y.-H. Chen, S.-C. Chen, Y.-Y. Lin, and W.-H. Peng, “MoTIF: Learning motion trajectories with local implicit neural functions for continuous space-time video super-resolution,” in *IEEE Conference on Computer Vision and Pattern Recognition*, 2023, pp. 23 131–23 141.
- [9] M. Haris, G. Shakhnarovich, and N. Ukita, “Space-time-aware multi-resolution video enhancement,” in *IEEE Conference on Computer Vision and Pattern Recognition*, 2020, pp. 2859–2868.
- [10] Y. Zhang, H. Wang, H. Zhu, and Z. Chen, “Optical flow reusing for high-efficiency space-time video super resolution,” *IEEE Trans. Circuits Syst. Video Technol.*, vol. 33, no. 5, pp. 2116–2128, 2023.
- [11] Y. Zhang, H. Wang, and Z. Chen, “Controllable space-time video super-resolution via enhanced bidirectional flow warping,” in *IEEE International Conference on Visual Communications and Image Processing*, 2022.
- [12] Z. Li, N. B. Kovachki, K. Azizzadenesheli, B. Liu, K. Bhattacharya, A. M. Stuart, and A. Anandkumar, “Neural operator: Graph kernel network for partial differential equations,” *arXiv preprint arxiv:2003.03485*, 2020.
- [13] J. Guibas, M. Mardani, Z. Li, A. Tao, A. Anandkumar, and B. Catanzaro, “Adaptive fourier neural operators: Efficient token mixers for transformers,” *arXiv preprint arxiv:2111.13587*, 2021.
- [14] G. Wen, Z. Li, K. Azizzadenesheli, A. Anandkumar, and S. M. Benson, “U-FNO - an enhanced fourier neural operator based-deep learning model for multiphase flow,” *arXiv preprint arxiv: 2109.03697*, 2021.
- [15] A. H. d. O. Fonseca, E. Zappala, J. O. Caro, and D. van Dijk, “Continuous spatiotemporal transformers,” *arXiv preprint arXiv:2301.13338*, 2023.
- [16] Z. Li, N. B. Kovachki, K. Azizzadenesheli, B. Liu, K. Bhattacharya, A. M. Stuart, and A. Anandkumar, “Fourier neural operator for parametric partial differential equations,” in *International Conference on Learning Representations*, 2021.
- [17] P. Constantin and C. Foias, *Navier-stokes equations*. University of Chicago press, 1988.
- [18] A. Tran, A. P. Mathews, L. Xie, and C. S. Ong, “Factorized fourier neural operators,” in *International Conference on Learning Representations*, 2023.
- [19] W. Xiong, X. Huang, Z. Zhang, R. Deng, P. Sun, and Y. Tian, “Koopman

- neural operator as a mesh-free solver of non-linear partial differential equations,” *arXiv preprint arXiv:2301.10022*, 2023.
- [20] J. Liang, J. Cao, G. Sun, K. Zhang, L. V. Gool, and R. Timofte, “Swinir: Image restoration using swin transformer,” in *IEEE International Conference on Computer Vision*, 2021, pp. 1833–1844.
- [21] J. Cao, Q. Wang, Y. Xian, Y. Li, B. Ni, Z. Pi, K. Zhang, Y. Zhang, R. Timofte, and L. Van Gool, “CiaoSR: Continuous implicit attention-in-attention network for arbitrary-scale image super-resolution,” in *IEEE Conference on Computer Vision and Pattern Recognition*, 2023, pp. 1796–1807.
- [22] W. Bao, W.-S. Lai, C. Ma, X. Zhang, Z. Gao, and M.-H. Yang, “Depth-aware video frame interpolation,” in *IEEE Conference on Computer Vision and Pattern Recognition*, 2019, pp. 3703–3712.
- [23] Z. Huang, T. Zhang, W. Heng, B. Shi, and S. Zhou, “Real-time intermediate flow estimation for video frame interpolation,” *European Conference on Computer Vision*, pp. 624–642, 2022.
- [24] L. Kong, B. Jiang, D. Luo, W. Chu, X. Huang, Y. Tai, C. Wang, and J. Yang, “IFRnet: Intermediate feature refine network for efficient frame interpolation,” in *IEEE Conference on Computer Vision and Pattern Recognition*, 2022, pp. 1969–1978.
- [25] W. Shen, W. Bao, G. Zhai, L. Chen, X. Min, and Z. Gao, “Video frame interpolation and enhancement via pyramid recurrent framework,” *IEEE Trans. Image Process.*, vol. 30, pp. 277–292, 2021.
- [26] D. Li, Y. Liu, and Z. Wang, “Video super-resolution using non-simultaneous fully recurrent convolutional network,” *IEEE Trans. Image Process.*, vol. 28, no. 3, pp. 1342–1355, 2019.
- [27] P. Yi, Z. Wang, K. Jiang, Z. Shao, and J. Ma, “Multi-temporal ultra dense memory network for video super-resolution,” *IEEE Trans. Circuits Syst. Video Technol.*, vol. 30, no. 8, pp. 2503–2516, 2020.
- [28] K. C. Chan, X. Wang, K. Yu, C. Dong, and C. C. Loy, “BasicVSR: The search for essential components in video super-resolution and beyond,” in *IEEE Conference on Computer Vision and Pattern Recognition*, 2021, pp. 4947–4956.
- [29] W. Wen, W. Ren, Y. Shi, Y. Nie, J. Zhang, and X. Cao, “Video super-resolution via a spatio-temporal alignment network,” *IEEE Trans. Image Process.*, vol. 31, pp. 1761–1773, 2022.
- [30] M. Liu, S. Jin, C. Yao, C. Lin, and Y. Zhao, “Temporal consistency learning of inter-frames for video super-resolution,” *IEEE Trans. Circuits Syst. Video Technol.*, vol. 33, no. 4, pp. 1507–1520, 2023.
- [31] J. Dong, K. Ota, and M. Dong, “Video frame interpolation: A comprehensive survey,” *ACM Trans. Multim. Comput. Commun. Appl.*, vol. 19, no. 2s, pp. 1–31, 2023.
- [32] H. Liu, Z. Ruan, P. Zhao, C. Dong, F. Shang, Y. Liu, L. Yang, and R. Timofte, “Video super-resolution based on deep learning: a comprehensive survey,” *Artificial Intelligence Review*, vol. 55, no. 8, pp. 5981–6035, 2022.
- [33] S. Cao, “Choose a transformer: Fourier or galerkin,” in *Advances in Neural Information Processing Systems*, 2021, pp. 24 924–24 940.
- [34] M. Wei and X. Zhang, “Super-resolution neural operator,” in *IEEE Conference on Computer Vision and Pattern Recognition*, 2023, pp. 18 247–18 256.
- [35] A. Vaswani, N. Shazeer, N. Parmar, J. Uszkoreit, L. Jones, A. N. Gomez, L. Kaiser, and I. Polosukhin, “Attention is all you need,” in *Advances in Neural Information Processing Systems*, 2017, pp. 5998–6008.
- [36] P. Ren, C. Rao, Y. Liu, J.-X. Wang, and H. Sun, “PhyCRNet: Physics-informed convolutional-recurrent network for solving spatiotemporal pdes,” *Computer Methods in Applied Mechanics and Engineering*, vol. 389, p. 114399, 2022.
- [37] L. Lu, R. Wu, H. Lin, J. Lu, and J. Jia, “Video frame interpolation with transformer,” in *IEEE Conference on Computer Vision and Pattern Recognition*, 2022, pp. 3532–3542.
- [38] G. Zhang, Y. Zhu, H. Wang, Y. Chen, G. Wu, and L. Wang, “Extracting motion and appearance via inter-frame attention for efficient video frame interpolation,” in *IEEE Conference on Computer Vision and Pattern Recognition*, 2023, pp. 5682–5692.
- [39] A. Dosovitskiy, L. Beyer, A. Kolesnikov, D. Weissenborn, X. Zhai, T. Unterthiner, M. Dehghani, M. Minderer, G. Heigold, S. Gelly, J. Uszkoreit, and N. Houlsby, “An image is worth 16x16 words: Transformers for image recognition at scale,” in *International Conference on Learning Representations*, 2021.
- [40] X. Chen, X. Wang, J. Zhou, Y. Qiao, and C. Dong, “Activating more pixels in image super-resolution transformer,” in *IEEE Conference on Computer Vision and Pattern Recognition*, 2023, pp. 22 367–22 377.
- [41] S. Shi, J. Gu, L. Xie, X. Wang, Y. Yang, and C. Dong, “Rethinking alignment in video super-resolution transformers,” in *Advances in Neural Information Processing Systems*, 2022, pp. 36 081–36 093.
- [42] Y. Chen, S. Liu, and X. Wang, “Learning continuous image representation with local implicit image function,” in *IEEE Conference on Computer Vision and Pattern Recognition*, 2021, pp. 8628–8638.
- [43] H. Jiang, D. Sun, V. Jampani, M. H. Yang, and J. Kautz, “Super slo-mo: High quality estimation of multiple intermediate frames for video interpolation,” in *IEEE Conference on Computer Vision and Pattern Recognition*, 2018, pp. 9000–9008.
- [44] X. Wang, K. Chan, K. Yu, C. Dong, and C. C. Loy, “EDVR: Video restoration with enhanced deformable convolutional networks,” in *IEEE Conference on Computer Vision and Pattern Recognition Workshops*, 2019.
- [45] X. Cheng and Z. Chen, “Multiple video frame interpolation via enhanced deformable separable convolution,” *IEEE Trans. Pattern Anal. Mach. Intell.*, vol. 44, no. 10, pp. 7029–7045, 2022.
- [46] K. C. Chan, S. Zhou, X. Xu, and C. C. Loy, “BasicVSR++: Improving video super-resolution with enhanced propagation and alignment,” in *IEEE Conference on Computer Vision and Pattern Recognition*, 2022, pp. 5972–5981.
- [47] T. Xue, B. Chen, J. Wu, D. Wei, and W. T. Freeman, “Video enhancement with task-oriented flow,” *International Journal of Computer Vision*, vol. 127, no. 8, pp. 1106–1125, 2019.
- [48] C. Liu and D. Sun, “A bayesian approach to adaptive video super resolution,” in *IEEE Conference on Computer Vision and Pattern Recognition*, 2011, pp. 209–216.
- [49] S. Nah, T. H. Kim, and K. M. Lee, “Deep multi-scale convolutional neural network for dynamic scene deblurring,” in *IEEE Conference on Computer Vision and Pattern Recognition*, 2017, pp. 257–265.
- [50] X. Tao, H. Gao, R. Liao, J. Wang, and J. Jia, “Detail-revealing deep video super-resolution,” in *IEEE International Conference on Computer Vision*, 2017, pp. 4472–4480.
- [51] D. P. Kingma and J. Ba, “Adam: A method for stochastic optimization,” *arXiv preprint arXiv:1412.6980*, 2014.
- [52] W.-S. Lai, J.-B. Huang, N. Ahuja, and M.-H. Yang, “Deep laplacian pyramid networks for fast and accurate super-resolution,” in *IEEE Conference on Computer Vision and Pattern Recognition*, 2017, pp. 624–632.
- [53] S. Jiang, D. Campbell, Y. Lu, H. Li, and R. I. Hartley, “Learning to estimate hidden motions with global motion aggregation,” in *IEEE International Conference on Computer Vision*, 2021, pp. 9752–9761.
- [54] P. Fischer, A. Dosovitskiy, E. Ilg, P. Husser, C. Hazrba, V. Golkov, V. Patrick, D. Cremers, and T. Brox, “Flownet: Learning optical flow with convolutional networks,” in *IEEE International Conference on Computer Vision*, 2016, pp. 2758–2766.
- [55] Z. Teed and J. Deng, “RAFT: recurrent all-pairs field transforms for optical flow,” in *European Conference on Computer Vision*, 2020, pp. 402–419.
- [56] D. Sun, X. Yang, M.-Y. Liu, and J. Kautz, “Models matter, so does training: An empirical study of cnns for optical flow estimation,” *IEEE Trans. Pattern Anal. Mach. Intell.*, vol. 42, no. 6, pp. 1408–1423, 2018.
- [57] S. Niklaus and F. Liu, “Softmax splatting for video frame interpolation,” in *IEEE Conference on Computer Vision and Pattern Recognition*, 2020, pp. 5437–5446.
- [58] A. Ranjan and M. J. Black, “Optical flow estimation using a spatial pyramid network,” in *IEEE Conference on Computer Vision and Pattern Recognition*, 2017, pp. 4161–4170.
- [59] X. Li, J. Dong, J. Tang, and J. Pan, “Dlgsanet: lightweight dynamic local and global self-attention networks for image super-resolution,” in *IEEE International Conference on Computer Vision*, 2023, pp. 12 792–12 801.
- [60] X. Chen, X. Wang, J. Zhou, Y. Qiao, and C. Dong, “Activating more pixels in image super-resolution transformer,” in *IEEE Conference on Computer Vision and Pattern Recognition*, 2023, pp. 22 367–22 377.